IMMUNOLOGY

Mannan-induced Nos2 in macrophages enhances IL-17–driven psoriatic arthritis by innate lymphocytes

Jianghong Zhong,[1] Tatjana Scholz,[2] Anthony C. Y. Yau,[1] Simon Guerard,[1] Ulrike Hüffmeier,[3] Harald Burkhardt,[2] Rikard Holmdahl[1,4]*

Previous identification of the inducible nitric oxide synthase (NOS2) gene as a risk allele for psoriasis (Ps) and psoriatic arthritis (PsA) suggests a possible pathogenic role of nitric oxide (NO). Using a mouse model of mannan-induced Ps and PsA (MIP), where macrophages play a regulatory role by releasing reactive oxygen species (ROS), we found that NO was detectable before disease onset in mice, independent of a functional nicotinamide adenine dinucleotide phosphate oxidase 2 complex. MIP was suppressed by either deletion of Nos2 or inhibition of NO synthases with NG-nitro-L-arginine methyl ester, demonstrating that Nos2-derived NO is pathogenic. NOS2 expression was also up-regulated in lipopolysaccharide- and interferon-γ–stimulated monocyte subsets from patients with PsA compared to healthy controls. Nos2-dependent interleukin-1α (IL-1α) release from skin macrophages was essential for arthritis development by promoting IL-17 production of innate lymphoid cells. We conclude that Nos2-derived NO by tissue macrophages promotes MIP, in contrast to the protective effect by ROS.

INTRODUCTION

Mannan is a natural ligand for mannose receptors at the host-fungus interactions and is known as the major trigger of interleukin-17 (IL-17) pathways in the host (1, 2). Abundant mannans are found in nearly all fungi, of which the most common, Saccharomyces cerevisiae and Candida albicans, have been described as pathogenic factors of intertriginous psoriasis (Ps) and psoriatic arthritis (PsA) (3) since the early 1980s (4). Nevertheless, the role of mannan has not yet been fully addressed.

Ps has been widely regarded as immune-mediated disease of the skin that is associated in approximately one-third of the patients with the development of PsA. Ps is a heterogeneous chronic disease driven by major histocompatibility complex (MHC)–restricted T cells operating through the IL-17/IL-22/IL-23 signaling pathway (5). This traditional view of Ps is supported by the strong association with the HLA-C*0602 allele (6). However, conditional analysis of large case control data sets uncovered additional Ps risk alleles in loci encoding nonclassical MHC class I molecules (6). These data and more recent results from murine experimental models of Ps (7), as well as human studies demonstrating the presence of various types of innate T cells in psoriatic skin (8), suggest that these innate effectors play important roles in psoriatic plaque formation. Classical αβ T cells and various types of innate T cells may secrete IL-17 and be closely involved in the pathogenic IL-17 pathways. Recent clinical studies on blocking agents of various steps in the IL-17 pathway have demonstrated its crucial role in both Ps and PsA (5), but the triggering mechanisms and modifiers, as well as involvements of different T cell types, have not yet been clarified.

Besides the strong influence of the MHC region, a locus containing the inducible nitric oxide synthase (NOS2) gene is associated with Ps and PsA susceptibility (9, 10). Nos2 expression and production of nitric oxide (NO) can be induced in murine macrophages after stimulation with lipopolysaccharide (LPS) (11). Similar to LPS, a diversity of ligands

interacts with mannose receptors on macrophages, including mannan derived from S. cerevisiae. Thus, it is possible that agents such as mannan could activate tissue macrophages, activate NO production, and trigger the development of Ps and PsA.

Recent findings in animal models of Ps, such as both the imiquimod-induced (7) and mannan-induced (2) diseases, all argue for a prominent role of IL-17–producing innate lymphocytes rather than MHC-restricted αβ T cells. Injection of mannan into certain mouse strains induces a disease that is remarkably similar to Ps and PsA in humans, that is, the mannan-induced Ps and PsA (MIP) model (2). The MIP model is independent of αβ T cells and is associated with activation of macrophages that triggers the production of IL-17A by innate lymphocytes (2, 12).

The disease of MIP is more severe in mouse strains carrying a mutation in the neutrophil cytosol factor 1 (Ncf1) gene (2). The Ncf1 mutation impairs superoxide anion production by the nicotinamide adenine dinucleotide phosphate oxidase 2 (NOX2) complex (13, 14). Generation of superoxide anion eventually leads to a cascade of the other reactive oxygen and nitrogen species (ROS/RNS), such as hydrogen peroxide, hydroxyl radical, NO, and peroxynitrite. Many diseases have been linked to damage from ROS as a result of an imbalance between radicals generating and their elimination by protective mechanisms referred to as antioxidants (14). This prevailing paradigm was challenged by a hypothesis-free study searching for the polymorphic genes controlling chronic inflammation in rats (14), and the positional cloning of the disease-promoting allele of the Ncf1 gene showed that ROS regulates rather than promotes disease. Ncf1 mutations in mice and humans (15) confirmed the findings in rats. However, despite the recent advances on the role of ROS/RNS, many challenges remain, and future studies should focus on the role of NO in inflammatory pathways.

Here, we investigated the role of RNS in MIP development by administration of NO synthases inhibitor NG-nitro-L-arginine methyl ester (L-NAME) in combination with Nos2-deficient mice of both $Ncf1^{+/+}$ and $Ncf1^{*/*}$ mouse strains. To noninvasively monitor the effect of inhibiting Nos2 in mice, we used optical tomography imaging (16) to visualize RNS using the probe L-012 (17). These results and the phenotypic characterization of the cellular infiltrates show that mannan-induced Nos2 activation and IL-1α release from skin macrophages

[1]Medical Inflammation Research, Department of Medical Biochemistry and Biophysics, Karolinska Institutet, Stockholm 171 77, Sweden. [2]Project Group Translational Medicine and Pharmacology, Fraunhofer Institute for Molecular Biology and Applied Ecology and Division of Rheumatology, University Hospital Frankfurt, Goethe University, Frankfurt am Main 605 90, Germany. [3]Institute of Human Genetics, Friedrich-Alexander-Universität Erlangen-Nürnberg, Erlangen 910 54, Germany. [4]School of Pharmaceutical Sciences, Southern Medical University, Guangzhou, China.
*Corresponding author. Email: rikard.holmdahl@ki.se

are essential for MIP disease development by innate lymphoid cells. A concomitant analysis revealed an increased NOS2 up-regulation in LPS- and interferon-γ (IFN-γ)–challenged monocyte subpopulations derived from the blood in PsA patients compared to those obtained from healthy donors (HDs), thereby suggesting the potential relevance of the uncovered pathogenic role of NO in MIP also for psoriatic disease in humans.

RESULTS

NO is induced by mannan and contributes to the development of psoriatic disease

We previously demonstrated that macrophage-restricted, NOX2-induced superoxide anion, together with other ROS molecules, suppresses MIP (2). In addition to ROS, other radicals and reactive molecules, such as RNS including three variants of NO ($NO^{\cdot}/NO^{+}/NO^{-}$), could also be generated from murine macrophages under inflammatory conditions. Therefore, we examined the level of serum NO_x (nitrate and nitrite) in both Ncf1 wild-type ($Ncf1^{+/+}$) and Ncf1 mutation ($Ncf1^{*/*}$) mice injected with mannan. At day 5 after mannan injection, we found that NO production increased in both $Ncf1^{*/*}$ mice

and $Ncf1^{+/+}$ controls (Fig. 1). Similar to previous studies, ROS-deficient $Ncf1^{*/*}$ mice developed more severe disease compared with $Ncf1^{+/+}$ mice (2). Remarkably, the concentration of serum NO_x was higher in $Ncf1^{*/*}$ mice than that in wild-type $Ncf1^{+/+}$ controls (Fig. 1A). Together, these findings suggest that NO production can be induced by mannan and that more RNS is observed when NOX2 produces less ROS.

We next investigated the level of circulating NO triggered by mannan injection and the effect of NO synthase inhibition. To achieve this, we injected mice with L-NAME, and used mice injected with the less-active isomer NG-nitro-D-arginine methyl ester (D-NAME), as well as those injected with phosphate-buffered saline (PBS), as controls. Figure 1B shows the level of RNS in serum over the period of 24 hours following L-NAME or PBS injection at days 2 and 5 after mannan injection, respectively. Eight hours after injection of L-NAME, we observed a significant reduction of RNS in serum. However, this effect was gone 12 hours after L-NAME injection, indicating a very short-lived effect. We therefore decided to treat the mice with daily administrations of L-NAME, although this could give intermittent peak effects.

To monitor the long-term effect of NO depletion, we performed in vivo optical imaging of the production of peroxynitrite, which is
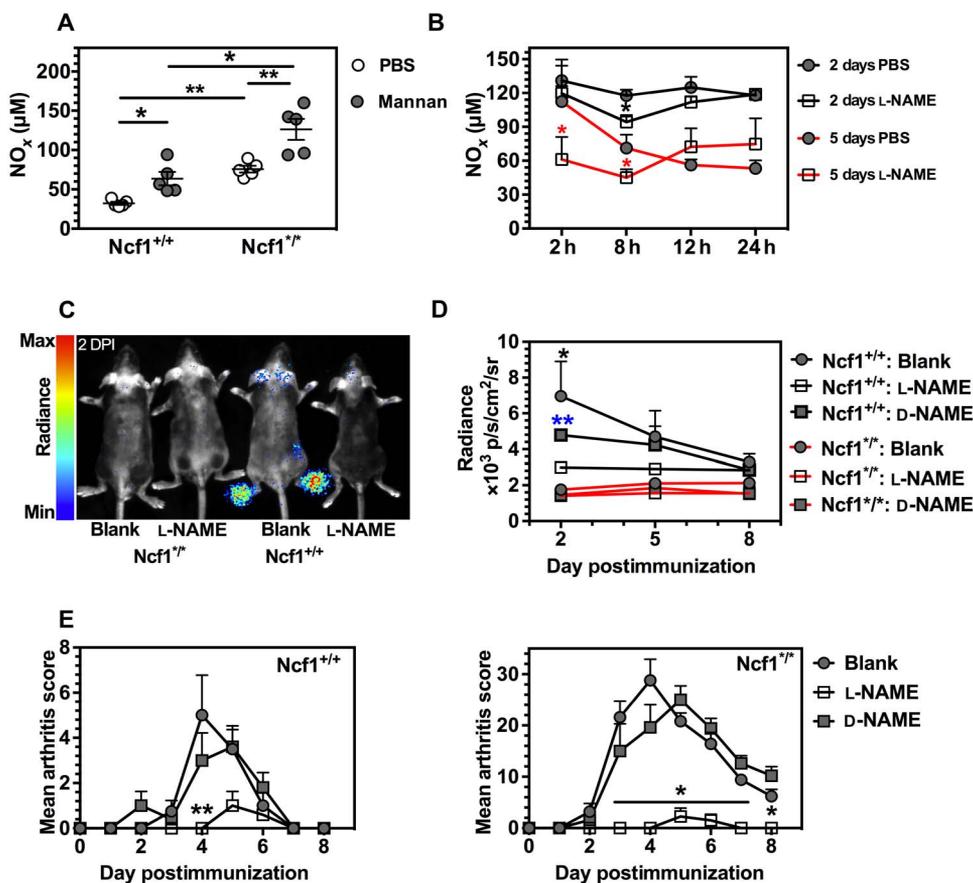

Fig. 1. Mannan induces the production of NO. (**A**) The serum NO_x status in $Ncf1^{+/+}$ and $Ncf1^{*/*}$ mice at day 5 after mannan administration (n = 5). Phosphate-buffered saline (PBS) injection was used as negative controls (n = 5). (**B**) Kinetic effect of L-NAME administration on serum NO_x status in $Ncf1^{*/*}$ mice at 2 and 5 days postinjection (DPI) of mannan using PBS as controls. n = 5 mice per group. The black asterisk stands for the significance in comparison at 2 DPI, whereas the red one for 5 DPI. (**C**) Example of in vivo peroxynitrite imaging at 2 DPI. (**D**) Statistical analysis of the mean optical radiance at paws per mouse at 2, 5, and 8 DPI. The significance is calculated for each control group in comparison with the L-NAME group. (**E**) Suppression of mannan-induced Ps-like arthritis by administration of L-NAME. The asterisk stands for the significance comparing L-NAME group with the D-NAME and blank group. For (D) and (E), both $Ncf1^{+/+}$ and $Ncf1^{*/*}$ mice were divided into three groups (n = 5 per group), that is, L-NAME and D-NAME treatments and nontreated individuals as blank controls. All results are shown as mean ± SEM.

the primary product in the reaction between NO and superoxide, and thus gives an indirect measure of NO status. The principle of this in vivo imaging is that a free radical reaction of peroxynitrite with L-012 results in luminescence (18). The chemiluminescent signal intensity is quantified as the average radiance within a region of interest (ROI) over time to determine the concentration of peroxynitrite. To reduce the motion artifacts and to reduce absorption and blocking of photon emission by black hair during the whole-body scanning, we anesthetized and shaved the mice before imaging. Figure 1C shows a representative image of peroxynitrite production. We found that luminescence mainly occurred in the paws and toes, and only a few photons were emitted from ears. The mean radiance of the paws in $Ncf1^{+/+}$ mice with L-NAME injection was lower than those with D-NAME treatment or without any L-NAME/D-NAME treatment as blank controls on day 2 postinjection (2 DPI) of mannan (Fig. 1D). There was no detectable optical emission in the $Ncf1^{*/*}$ mice, which confirmed that production of mannan-induced peroxynitrite is dependent on the NOX2-derived superoxide. In MIP disease, the skins around ears and paws are areas that are the most prominently inflamed (2). The observed tissue-specific production of NO correlated with the severity of the local skin lesions.

Finally, we addressed the role of the NO synthase inhibitor L-NAME in controlling MIP disease development, manifested by both skin and joint affections, herein referred to as Ps and PsA, respectively, and whether such an effect is dependent on Ncf1. $Ncf1^{+/+}$ and $Ncf1^{*/*}$ mice were injected with mannan at day 0 and were treated daily with L-NAME or D-NAME, whereas mannan-injected mice without any treatment were used as blank controls. All the mice were observed for 8 days after mannan injection. At 4 DPI, a significant reduction of MIP disease in the skin around the paws was observed in $Ncf1^{+/+}$ mice treated with L-NAME (Fig. 1E). The $Ncf1^{*/*}$ mice developed more severe MIP than $Ncf1^{+/+}$ mice, as expected, which was effectively suppressed by L-NAME treatment (Fig. 1E). These results show that blocking NO was effective in protecting against MIP in both $Ncf1^{+/+}$ and $Ncf1^{*/*}$ mouse strains.

Deficiency of Nos2 alleviates MIP disease

To understand the role of NO in ROS-influenced environments and address the contribution of Nos2 activity to disease susceptibility, we backcrossed a null allele of Nos2 (19) into $C57BL/6N.Q.Ncf1^{*/*}$ by more than five generations, after which experiments were performed on intercrossed littermates. We evaluated the effect of L-NAME and Nos2 deficiency on the level of NO_x in serum on day 5 after mannan injection (peak of MIP), in both $Ncf1^{+/+}$ and $Ncf1^{*/*}$ mouse strains (Fig. 2A). First, we showed that there was no difference in serum NO production in the naïve Nos2-deficient and Nos2-sufficient mice. After mannan injection, the level of NO_x in serum of Nos2-deficient mice, at a comparable level of the wild-type mice with L-NAME treatment, was lower than that in the wild-type littermates with PBS treatment (Fig. 2A, left). This result shows that Nos2-derived NO was the main source of serum NO_x induced by mannan. Furthermore, a similar effect of
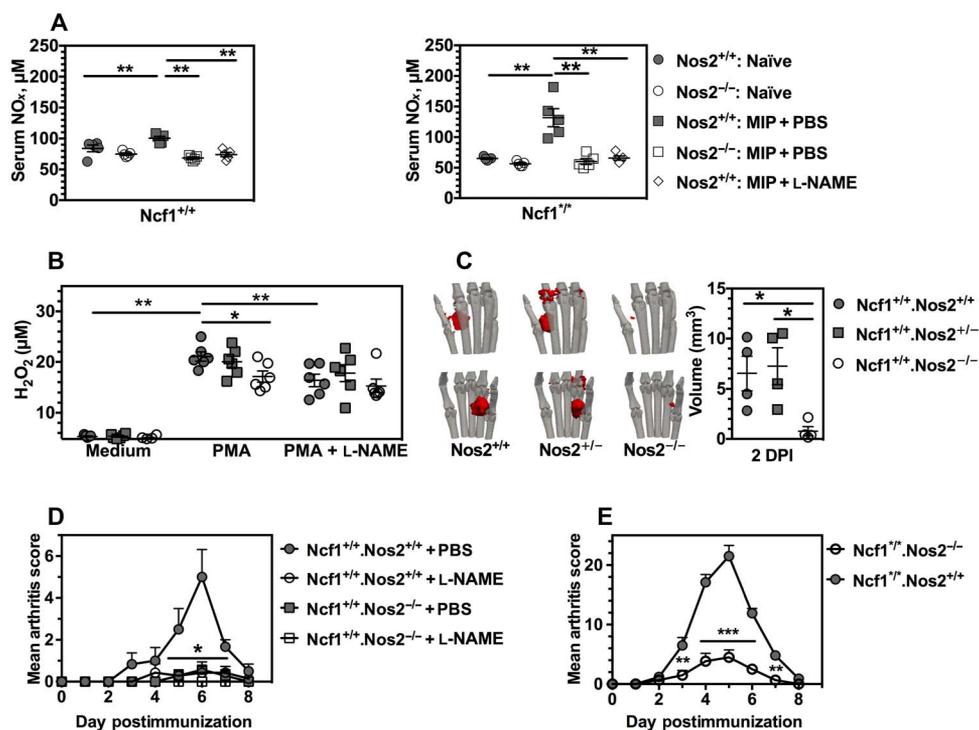
Fig. 2. Deficiency of Nos2 alleviates MIP development. (A) Levels of serum NO_x in naïve $Ncf1^{+/+}.Nos2^{-/-}$ mice and the $Ncf1^{+/+}.Nos2^{+/+}$ littermates and naïve $Ncf1^{*/*}.Nos2^{-/-}$ mice and their littermates $Ncf1^{*/*}.Nos2^{+/+}$ mice, compared with serum NO_x at 5 DPI. L-NAME was administered daily for 5 days beginning on day 0, and PBS was used as the control (n = 5 mice per group). (B) Comparison of H_2O_2 generation by fresh bone marrow cells isolated from naïve $Ncf1^{+/+}.Nos2^{-/-}$ mice, naïve littermates $Ncf1^{+/+}.Nos2^{+/-}$, and $Ncf1^{+/+}.Nos2^{+/+}$ controls under the defined conditions (n = 5 mice per group). (C) Representative tomography of peroxynitrite distribution (red volume) in the paw and the statistical comparison with the volume of peroxynitrite production in mice with genotype of $Ncf1^{+/+}.Nos2^{+/+}$ (n = 4), $Ncf1^{+/+}.Nos2^{+/-}$ (n = 4), and $Ncf1^{+/+}.Nos2^{-/-}$ (n = 4) at 2 DPI. In (B) and (C), the same marked signs stand for these three kinds of mice groups. (D) Evaluation of the effect of L-NAME in both $Ncf1^{+/+}.Nos2^{-/-}$ and the littermate $Ncf1^{+/+}.Nos2^{+/+}$ mice after mannan injection (n = 7 mice per group). (E) A study of arthritis was performed in both $Ncf1^{*/*}.Nos2^{-/-}$ mice (n = 6) and the littermate $Ncf1^{*/*}.Nos2^{+/+}$ mice (n = 10) after mannan injection. All results are shown as mean ± SEM.

Nos2 deficiency was observed in the wild-type mice, suggesting that the role of Nos2 is independent of Ncf1 (Fig. 2A, right).

Because ROS has been shown to be protective in MIP (*2*), we next examined whether the *Nos2* deficiency increased H_2O_2 production. Bone marrow cells were isolated from the naïve $Ncf1^{+/+}.Nos2^{-/-}$ mice, $Ncf1^{+/+}.Nos2^{+/-}$ mice, and their littermates ($Ncf1^{+/+}.Nos2^{+/+}$ controls) and were then stimulated with phorbol 12-myristate 13-acetate (PMA) in the absence or presence of L-NAME. Both *Nos2* deficiency and L-NAME treatment resulted in a lower level of PMA-induced H_2O_2 production (Fig. 2B).

To monitor the in vivo peroxynitrite production, we injected $Nos2^{-/-}$, $Nos2^{+/-}$, and $Nos2^{+/+}$ littermate mice with mannan at day 0 and then performed optical scanning at 2 DPI. Using the four-view optical planar imaging, we reconstructed the three-dimensional (3D) tomography of in vivo peroxynitrite distribution within the hind paw and quantified the inverse reconstructed volume of optical source (Fig. 2C). The *Nos2*-deficient mice gave a smaller chemiluminescence signal, reflecting a reduced production of peroxynitrite in the paw compared with wild-type controls.

We next investigated the effect of *Nos2* deficiency and L-NAME treatment on MIP. We found that both *Nos2* deficiency and L-NAME treatment resulted in a reduction of the clinical scores (Fig. 2D). After having demonstrated a protective effect of *Nos2* deficiency in wild-type mice, we investigated the effect of NO in a reduced environment using $Ncf1^{*/*}.Nos2^{-/-}$ and $Ncf1^{*/*}.Nos2^{+/+}$ mice. We found that deficiency of *Nos2* similarly resulted in lower clinical scores in *Ncf1*-deficient mice (Fig. 2E), as well as reduced the thickness of hind ankles and ears. Thus, NO derived from Nos2 plays an important role in enhancing MIP severity regardless of a functional Ncf1.

NOS2 expression is increased in CD14$^+$ PBMCs from PsA patients

So far, we have shown that macrophage-restricted Ncf1 expression (*13*) and superoxide production, partially neutralizing NO into peroxynitrite, restore arthritis resistance to the level of wild-type mice in the MIP model (*2*). This suggests that monocytes and macrophages can be essential sources of NOS2-dependent pathways behind the development of PsA in humans. To address whether this is the case, we measured the levels of expression of NOS2, as determined by the mean fluorescence intensities (MFIs) of NOS2 using flow cytometry, in different subpopulations of human peripheral blood mononuclear cells (PBMCs) from patients with PsA and HDs. The flow cytometry–gating strategy of PBMCs and NOS2 analysis is shown in fig. S1. We found an up-regulation of NOS2 MFIs in the LPS- and IFN-γ–stimulated CD14$^+$ monocyte subpopulation in patients with PsA compared with HDs (Fig. 3). In addition, we investigated a cell subset representing a unique CD11c$^+$ dendritic cell phenotype that is abundantly detectable in inflamed tissue (for example, psoriatic skin) and referred to as tumor necrosis factor–α (TNF-α)– and NOS2-producing dendritic cells (TIP DCs) (*20*). Upon in vitro differentiation of the TIP DCs from CD14$^+$ PBMC populations according to the described method (*21*), flow cytometric characterizations did not reveal significant differences in the level of NOS2 expression between PsA- and HD-derived cells in response to the above-mentioned LPS and IFN-γ challenge (Fig. 3). Myeloid-derived suppressor cells (MDSCs) are regarded as a heterogeneous NOS2-expressing cell population involved in limiting inflammation via the suppression of T cell responses, although proinflammatory MDSC subsets with their capacity to drive T helper 17 cell differentiation was described in collagen-induced arthritis and rheumatoid arthritis (RA)
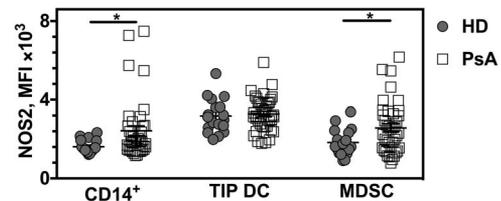

Fig. 3. NOS2 expression is enhanced upon in vitro activation for patients with PsA. Following an identical IFN-γ and LPS preactivation procedure, MFIs of NOS2 expression in CD14$^+$ PBMC subpopulation (CD14$^+$), human leukocyte antigen–DR (HLA-DR) and CD11c double-positive cells (TIP DC), and CD11b$^+$ MDSC subpopulation were determined in the cohort of PsA patients ($n = 39$), compared with those obtained in the HD group ($n = 18$). All results are shown as mean ± SEM.

(*22*). We also analyzed the CD11b$^+$-MDSC subpopulation (MDSC10 phenotype, Lin$^-$HLA-DR$^-$CD11b$^+$) (*23*) for NOS2 expression upon the same stimulus and detected higher levels in cells derived from PsA patients compared to those obtained from HDs (Fig. 3).

Nos2-dependent IL-1α promotes MIP disease

To understand the primary downstream signaling pathways of NO activity in MIP disease, we studied the cell and cytokine profiles of skin cells at the paw and toes at 5 DPI of mannan. We found that more than 80% of CD45$^+$ live skin cells were CD11b$^+$. The increase in the number of CD45$^+$CD11b$^+$ live skin cells after mannan injection could possibly explain the increased severity of paw inflammation in $Ncf1^{*/*}$ mice compared with $Ncf1^{+/+}$ mice. However, daily L-NAME treatment had no effect on the number of CD11b$^+$CD45$^+$ skin cells in comparison with PBS treatment (Fig. 4A).

We next cultured skin cells with PMA and ionomycin for 4 hours and studied the level of key proinflammatory cytokines in the culture supernatant. Because MIP is an IL-17–dependent disease regulated by TNF-α (*2*), we determined the concentration of TNF-α and IL-17 in the culture supernatant (Fig. 4, B and D). In addition, because neutrophil depletion blocks the MIP disease (*2*) and NOX2 has been suggested to control the neutrophilic response by IL-1α (*24*), we also determined the concentration of IL-1α in the culture supernatant (Fig. 4D). We found that L-NAME reduced the levels of IL-1α, TNF-α, and IL-17A at 5 DPI. In particular, *Nos2* deficiency resulted in a reduction of IL-1α to a level comparable to that of naïve mice (Fig. 4E). This suggests that resident IL-1α production depends on Nos2-derived NO. We further demonstrated the importance of IL-1α by showing that IL-1α neutralization reduced arthritis severity in $Ncf1^{*/*}$ mice (Fig. 4F). We conclude that NO-dependent IL-1α production is critical for MIP development.

NO is required for IL-17A production of ILC3

It is well known that IL-1R1 is expressed in type 3 innate lymphoid cells (ILC3) and γδ T cells, resulting in an IL-1α–triggered feedback loop involving IL-17 production at early phases of sterile inflammation (*25*). It is also known that αβ T and B cells are redundant in MIP disease induction (*2, 12*). We thus investigated whether ILC3 or γδ T cell is the cell subset responsible for the reduced IL-17A secretion when blocking endogenous NO synthesis in MIP. We injected $Ncf1^{*/*}$ mice with mannan at day 0, followed by daily administration of L-NAME or PBS. Figure 5A shows representative images of paws at 5 DPI. We found that L-NAME treatment suppressed the CD45$^+$ cell infiltration into the skin around the paw in MIP (Fig. 5B). However, the number of neither ILC3 nor γδ T cells was affected by L-NAME treatment. This suggests that the increased concentrations of IL-1α and IL-17A in MIP (Fig. 4, C and D)
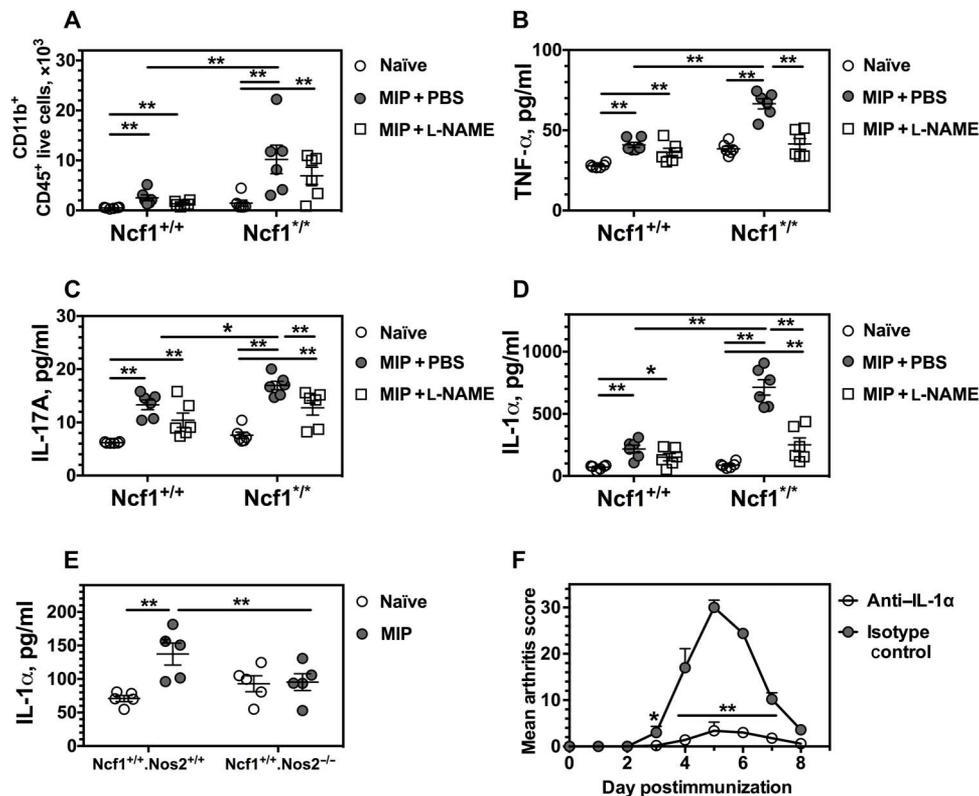
Fig. 4. NOS2-dependent IL-1α promotes MIP development. (**A**) The numbers of CD11b+CD45+ live skin cells were calculated for hind paws from both $Ncf1^{+/+}$ and $Ncf1^{*/*}$ mice with L-NAME or PBS treatment at 5 DPI. $n = 6$ mice per group including the naïve mice. (**B** to **D**) The concentrations of TNF-α, IL-17A, and IL-1α in the supernatant solution of skin cells were quantified after 4 hours of stimulation with PMA/ionomycin. (**E**) The NOS2-dependent increase of IL-1α was found in the supernatant of skin cells from the mice with MIP disease at day 5, and each group included five mice for the cytokine analysis. (**F**) Evaluation of the time course was performed in $Ncf1^{*/*}$ mice during IL-1α in vivo neutralization ($n = 5$ mice per group) after mannan injection. All results are shown as mean ± SEM.
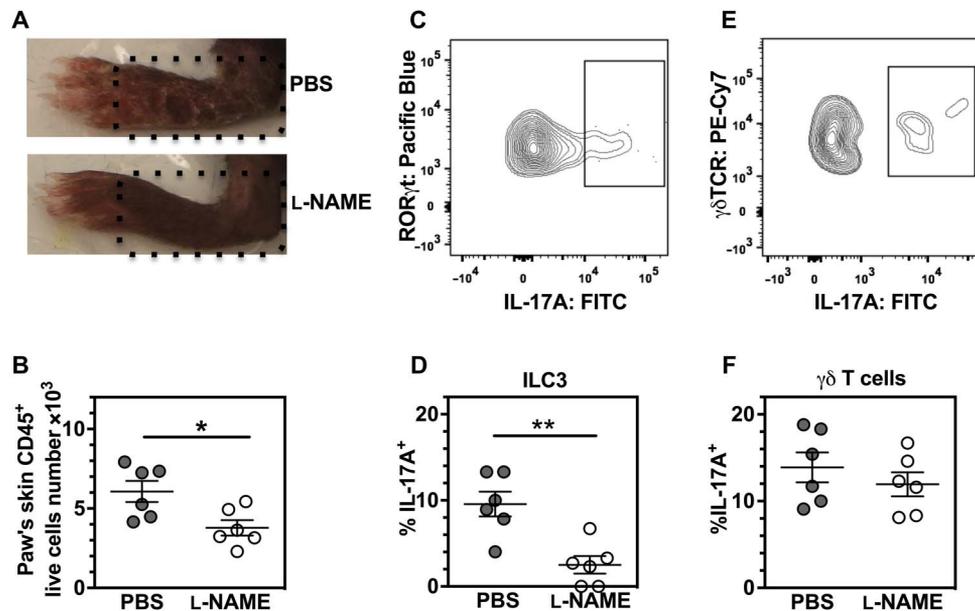

Fig. 5. Resident IL-17A production requires NO for ILC3 but not γδ T cells. The $Ncf1^{*/*}$ mice received an arthritogenic dose of mannan at day 0. L-NAME and PBS were injected intraperitoneally daily for 5 days beginning on day 0, and the local skin was excised from hind paws when the mouse was sacrificed using CO_2 at day 5. The skin cells were analyzed by flow cytometry for the following cell populations: (i) total number of CD45+ live cells, (ii) CD45+CD3−CD90.2+CD127+RORγt+ live cells (ILC3), and (iii) CD45+βTCR−γδTCR+ live cells (γδ T cells). (**A**) Schematic illustration of the region of interest (ROI) at the position corresponding to dotted lines for isolating skin samples from the paw. (**B**) Number of CD45+ live skin cells from the selected ROI in the paw. (**C** to **F**) Frequency of IL-17A+ expression was shown within both ILC3 in (C) and (D) and γδ T cells in (E) and (F). Each group included five mice for the intracellular cytokine analysis by flow cytometry. All results are shown as mean ± SEM. Cy7, Cyanine7.

Table 1. Optical parameters of tissues at 535 nm with unit of mm^{-1}.

	Bone	Skin	Subcutaneous tissue
Absorption coefficient	0.01	0.71	0.10
Reduced scattering coefficient	2.18	4.18	1.73

could not be explained by an increase in the total numbers of ILC3 or γδ T cells. Nevertheless, we found that L-NAME treatment reduced the frequency of the IL-17A$^+$ subset of ILC3 cells in the skin (Fig. 5, C and D, and fig. S2) but had no effect on the frequency of IL-17A$^+$ γδ T cells in the skin of either *Ncf1$^{+/+}$* or *Ncf1$^{*/*}$* mice (Fig. 5, E and F, and fig. S3). These results indicate that the observed mannan-induced increase of NO-dependent IL-17A production was restricted to a subset of ILC3 cells but not to γδ T cells in the skin cell population.

DISCUSSION

The causes of Ps and PsA are unknown, although the exposure of the fungal moiety mannan is associated with psoriatic disease (*4*). In a mouse model of Ps and PsA induced by mannan, we found increased levels of NO in the local tissues (skin and paws) before clinical disease onset. We further demonstrated that superoxide and NO play contrasting roles in regulating MIP. NO generation by local macrophages leads to IL-1α release, which then activates ILC3 to produce IL-17A, resulting in enhanced disease severity.

Our findings may be of relevance in understanding the importance of ROS and RNS as signaling molecules that are critical factors in the development of autoimmune diseases. Superoxide anion is often referred to as the primary source of ROS with the potential to cause cellular damages, by interacting with other molecules to generate secondary free radicals in animals, such as NO-dependent reactions that produce RNS (*26*). However, previous studies showed that impaired ROS production is associated with more severe disease in MIP (*2*). An interesting question would now be to demonstrate whether NO could be protective in autoimmune diseases, similar to macrophage-derived ROS (*13, 14*). Here, we demonstrate that injection of mannan in mice activates skin cells to produce TNF-α, IL-1α, and IL-17A, which could mediate NO production by Nos2 in local macrophages within a positive feedback loop. Herein, we show that NO is pathogenic in the development of MIP and that the pathogenicity was dependent on NOS2 activation.

To our knowledge, MIP is the only known model for both Ps and PsA that is induced by a defined stimulus given systemically. Mannan activates certain pathways of the innate immune system through triggering of a large but limited number of receptors on inflammatory cells. In our MIP protocol, mannan was administrated intraperitoneally, and it is likely that the first encounter with macrophages or neutrophils occurs in the peritoneum. We observed a remarkable increase in the number of macrophages and neutrophils in the peritoneal cavity after administration of mannan. However, whether and how mannan interacts with neutrophils and macrophage is currently unclear. In vivo magnetic resonance imaging has shown the recognition and uptake of mannan by peritoneal macrophages (*27*). It is possible that mannan binds to several of the mannose receptors on macrophages. Dectin-2 is known as one of the mannose receptors, which are expressed on macrophages, and ligation of dectin-2 on RAW264.7 macrophages has been reported to trigger secretion of TNF-α (*28*). Another is the

macrophage mannose receptor (CD206) that could play a counteractive role in MIP (*29*), illustrating the high level of complexity of mannan perception by different receptors of the innate immune system that is likely cell type–specific and dependent on the environmental context.

Here, we found that IL-1α, TNF-α, and IL-17A were produced by skin cells in mice after mannan injection. Brody and Durum (*30*) found that an IL-1α precursor anchored to the plasma membrane of macrophages via a mannose receptor. Our results show that mannan triggered IL-1α release from macrophages. This concurs with published data confirming macrophages as primary sources of IL-1α production (*31*), with neutrophils as important downstream target cells in animals (*24*). In addition, type II IL-1 receptor on neutrophils was reported to suppress the progression of collagen-induced arthritis through the inhibition of IL-1 action on macrophages (*32*), suggesting that there is a direct regulatory loop between macrophages and neutrophils by the IL-1α pathway during the inflammatory process.

On the basis of our data, NO was found to be essential for extracellular IL-1α release. It is known that mRNA expression and protein levels of IL-1α affect the intracellular NO status in macrophages and NO can, in turn, modify both intra- and extracellular levels of IL-1α (*33*). After injection of mannan, the increase of NO in serum is associated with a high release of IL-1α from the local skin. *Nos2* deficiency abrogated the increase of IL-1α production in mice after injection of mannan. Besides neutrophils, ILC3 and γδ T cells are known to express IL-1 receptors and are also involved in the development of Ps (*8*) and arthritis (*34*). Therefore, we examined the effect of IL-1α on the activation of both ILC3 and γδ T cells. In the case of *Ncf1$^{*/*}$* mice, we showed that the frequency of IL-17A–producing cells is NO and IL-1α signaling–dependent in the skin ILC3 population but not in the γδ T cells population. In contrast to our previous result that neutralization of IL-1β did not affect the clinical outcome (*2*), IL-1α inhibition reduced the disease of MIP. IL-1 inhibition has also been investigated in the imiquimod-induced Ps model; the locally induced skin inflammation was partially reduced in mice deficient for both *IL-1α/IL-1β* but not in *IL-1α*– or *IL-1β*–deficient mice (*35*). Clinical trials using a human monoclonal antibody specific for IL-1α for Ps treatment have not reached general acceptance but have shown a promising therapeutic response in patients with Ps (*36*). Furthermore, low and high levels of IL-1α release control different bioavailability and roles in the nearby cell-cell interactions through IL-1 receptors compared with the secreted isoform that activates the downstream-targeted cells in a noncell contact signaling model. Thus, IL-1α inhibition is possibly effective in subtypes of Ps. In septic arthritis or in RA for comparison, therapeutic benefit was not observed for treatments with anakinra, a recombinant human IL-1 receptor antagonist (*37*). In the case of PsA, prospective, multicenter, randomized controlled trials with IL-1α–neutralizing agents are missing. However, a single open-label trial with anakinra performed in 20 PsA patients at a single center for 24 weeks showed 50 to 70% improvement of arthritis activity in 30% of responders (*38*), suggesting a therapeutic potential for IL-1 neutralization in a subgroup of this heterogeneous disease. In summary, these preclinical and clinical studies suggest that the IL-1α regulatory network varies among different disease conditions in skin and joints, and IL-1α may play a causative role in the IL-17–dependent disease upon triggering by selected stimuli.

Both cell-extrinsic ("triggers," that is, exogenous NO delivered by neighboring myeloid cells) and cell-intrinsic ("sensors") NOS2-derived NO has been shown to display both stimulatory and suppressive properties, but these diverging results could be due to that different cell subtypes have been addressed. The functional role of

NOS2 on the IL-17–producing T helper cell phenotypes for chronic inflammation is still debated (*39*). However, it is a widely accepted hypothesis that psoriatic disease likely arises from an unexplored defect in innate immunity. A novel strategy is therefore necessary to study the functional interactions between IL-17A signaling and NOS2 activity, which requires the use of animal models that allow studies of a systemic induction of psoriatic disease.

In conclusion, we have demonstrated contrasting roles of superoxide and NO in the process of MIP. We provide evidence that the pathogenic IL-1α secretion from the local macrophages is regulated differently by *Nos2* and *Ncf1* genes, and consequently, the downstream target ILC3 is controlled by two separate processes leading to characteristic changes in their IL-17A production. Upon stimulation of mannan, the skin macrophages produce a higher amount of IL-1α in *Ncf1*-mutant mice deficient of superoxide production than in the wild-type controls. The Nos2-dependent release of IL-1α may directly activate the local innate lymphocytes because of the up-regulation level of IL-17A in a subset of skin ILC3. These results should lead to reconsideration of a widely used description of ROS/RNS as having a uniformed role in psoriatic diseases and in the immune system in general.

MATERIALS AND METHODS
Animals
Founder of *B10Q* (*C57/B10.Q/rhd*, *Ncf1*^{+/+}) mice, originally from J. Klein (Tubingen University), is maintained by R. Holmdahl laboratory as an inbred strain. A mutation in the *Ncf1* gene (m1j) (Ncf1 protein also denoted p47phox) in the *B10Q* mice, designated as *B10Q. Ncf1*[m1j/m1j] or *Ncf1*[*/*], impairs the expression of the *Ncf1* gene, thereby totally blocking the function of the NOX2 complexes. *Nos2*-deficient mice (*B6.129P2-NOS2*[tm1Lau/J]) were obtained from the Jackson Laboratory and were crossed to our *C57BL/6N.Q* mice to get the *C57BL/ 6NJ.Q.Nos2*^{−/−} mice (*Ncf1*^{+/+}.*Nos2*^{−/−}) with control *Ncf1*^{+/+}.*Nos2*^{+/+} and *Ncf1*^{+/+}.*Nos2*^{+/−} littermates in the experiments here. *C57BL/6NJ. Q.Nos2*^{−/−} mice were crossed with *C57BL/6N.Q.Ncf1*[*/*] mice to generate the *C57BL/6NJ.Q.Ncf1*[*/*].*Nos2*^{−/−} mice (*Ncf1*[*/*].*Nos2*^{−/−}) with control *Ncf1*[*/*].*Nos2*^{+/+} and *Ncf1*[*/*].*Nos2*^{+/−} littermates. The primers for *Nos2* genotyping were as follows: 5′-ACATGCAGAATGAG-TACCGG-3′ (common), 5′-TCAACATCTCCT GGTGGAAC-3′ (wild type), and 5′-AATATGCGAAGTGGACCTCG-3′ (mutant). All mice in this study expressed the H2[q] haplotype; experimental mice were male mice, unless specified otherwise. Mice were housed under specific pathogen–free conditions in individual ventilated cages with wood-shaving bedding, a paper napkin as enrichment, and in a climate-controlled environment having a 12-hour light/dark cycle. All of the experiments were carried out in 8- to 9-week-old littermates. Each adult mouse weighed approximately 25 g. Experimental groups were randomized and distributed among mixed cages. Evaluation of arthritis severity was performed blindly and double-checked between the treated and control groups for each experiment. The animal study protocols were approved by Stockholm regional animal ethics committee, Sweden (N490/12 and N35/16).

Antibodies
The following antimouse antibodies were purchased from BioLegend: CD45 [clone 30-F11; PerCP5.5 or phycoerythrin (PE)–Cyanine7], T cell receptor (TCR) β chain (clone H57-597; PerCP5.5), TCR γ/δ (clone GL3; PE-Cyanine7), CD11b (clone M1/70; Pacific Blue), F4/80 [clone BM8; allophycocyanin (APC) or PerCP5.5], CD127 (clone

A7R34; Brilliant Violet 605), CD90.2 (clone 30-H12; Alexa Fluor 488), and IL-17A [clone TC11-18H10.1; fluorescein isothiocyanate (FITC) or APC]. PE streptavidin and antibodies for CD16/CD32 (clone 2.4G2; purified), CD3ε (clone 145-2C11; PerCP5.5), Gr-1 (clone RB6-8C5; APC), and RORγt (clone Q31-378; Alexa Fluor 647 or BV421) were purchased from BD Pharmingen. Antibodies for TNF-α (clone TN3-19; PE-Cyanine7) and mouse anti-iNOS (clone 6/iNOS/ NOS Type II; FITC) antibodies were purchased from BD Transduction Laboratories.

The antihuman lineage cocktail, including CD3, CD14, CD16, CD19, CD20, and CD56 (clones UCHT1, HCD14, 3G8, HIB19, 2H7, and HCD56; APC), CD244 (clone C1.7; PE), CD11b (clone CBRM1/5; PerCP-Cy5.5), HLA-DR (clone L243; Brilliant Violet 785), CD14 (clone HCD14; Brilliant Violet 421), CD33 (clone P67.6; APC/Cy7), CD11c (clone 3.9; APC), CD80 (clone 2D10; PE-Cy7), and CD86 (clone IT2.2; Brilliant Violet 711), were purchased from BioLegend. Antibodies for human NOS2 (clone C-11; Alexa Fluor 488) were purchased from Santa Cruz Biotechnology.

Mannan-induced PsA
Mice were injected intraperitoneally with 20 mg of mannan from the yeast *S. cerevisiae* (M7504, Sigma-Aldrich) dissolved in 200 μl of PBS only on day 0. Mice were scored daily for inflammation in the peripheral joints; one point was given for each swollen and red toe or joint and five points for a swollen ankle, adding up to a maximum score of 60 points per mouse.

Blocking NO
Age-matched mice were administered intraperitoneally with 100-μl volume of L-NAME (Sigma-Aldrich), D-NAME (Sigma-Aldrich), or PBS. Both L-NAME and D-NAME were dissolved into PBS, respectively. The dose of L-NAME or D-NAME was 200 mg/kg/day per mouse, that is, 5 mg/day per mouse.

NOS2 expression in human PBMCs
Blood samples of patients diagnosed with PsA were collected in the Division of Rheumatology at the University Hospital Frankfurt with written informed consent and approval by the local ethics committee. All patients ($n = 39$) [females, 51.3%; males, 48.7%; mean age, 57.7 ± 14.9 (SD) years; disease duration, 12.8 ± 8.7 (SD) years] fulfilled the CASPAR (Classification Criteria for Psoriatic Arthritis) criteria for classification of PsA (*40*). Blood samples (buffy coats) of HDs were obtained from the German Red Cross Blood Donation Centre Frankfurt. PBMCs were isolated and cultivated in TexMACS medium (Miltenyi Biotec) and the penicillin-streptomycin solution (Pen/Strep; 1%).

For analysis of NOS2 expression in CD14^{+} monocytes and MDSCs [MDC10 according to Mandruzzato *et al.* (*23*)] by flow cytometry, 1.5×10^6 PBMCs/ml were stimulated with IFN-γ (100 ng/ml; ImmunoTools) and LPS (1 μg/ml; InvivoGen) overnight. Subsequently, cells were stained with Zombie Aqua for live/dead discrimination, anti-Lin antibody cocktail, anti-CD244, anti-CD11b, anti–HLA-DR, anti-CD14, and anti-CD33. After fixation, anti-NOS2 was stained intracellularly. For flow cytometry analyses, doublets and dead cells were excluded from PBMCs, and living cells (Zombie-negative) were gated on Lin- and HLA-DR–negative population (MDSCs). MFIs for NOS2^{+} detection were subsequently determined.

The protocol was described previously for in vitro differentiation of a unique CD11c^{+} dendritic phenotype abundantly detectable in psoriatic skin (*22*), which is referred to as TIP DCs. Briefly, CD14^{+} cells were

isolated from PBMCs with CD14 MicroBeads (Miltenyi Biotec) and differentiated into TIP DC in TexMACS medium (Miltenyi Biotec) and Pen/Strep (1%) by stimulation with granulocyte-macrophage colony-stimulating factor (GM-CSF; 50 ng/ml; ImmunoTools) and IL-4 (50 ng/ml; PeproTech). At day 2, medium was exchanged by TexMACS (Miltenyi Biotec) and Pen/Strep (1%) containing GM-CSF (50 ng/ml), IFN-γ (100 ng/ml; ImmunoTools), and LPS (1 μg/ml; InvivoGen). At day 6, cells were harvested and stained with anti-CD11c, anti-CD80, anti-CD14, anti-CD86, anti–HLA-DR, and anti-CD11b. After fixation, anti-NOS2 was stained intracellularly. For flow cytometry, doublets and dead cells were excluded from the in vitro–differentiated dendritic cell population, and living cells (Zombie-negative) were gated on HLA-DR and CD11c double-positive dendritic cells. The MFIs of NOS2$^+$ cells in this population were analyzed.

Neutralization of IL-1α
Age-matched mice were administered intraperitoneally twice (−1 and 1 days) with antimouse IL-1α ALF-161 monoclonal antibody (BioXCell) and isotype controls, that is, polyclonal Armenian hamster IgG (BioXCell). Antibodies were dissolved in PBS, and the usage of ALF-161 or isotype control was 0.5 mg/time per mouse.

In vivo optical imaging of IL-1α
In vivo optical imaging was performed using a PhotonIMAGER (Biospace Lab), including an intensified charge-coupled device camera, 510- to 560-nm/50-nm bandpass filter, and a 4-view module. The luminescent probe L-012 was purchased from Wako Chemical (Nordic Biolabs) and dissolved in water HiPerSolv CHROMANORM for high-performance liquid chromatography. For in vivo imaging, the mice were immobilized with intraperitoneal injection of both ketamine (50 mg/kg; Orion Corporation) and domitor (1 mg/kg; Orion Corporation) dissolved together in PBS (1×; Life Technologies Europe BV). The mice under anesthesia were scanned immediately after intraperitoneal injection of L-012 (1 mg per mouse) for 20 min. The mice were awoken using antisedan (1 mg/kg; Orion Corporation) at the end of each experiment.

Serum NO (NO$_2^-$/NO$_3^-$) detection
Blood (100 μl) from the mouse-tail vein was taken to measure serum nitrite/nitrate levels. The tubes were kept for 15 min with gentle shaking and centrifuged at 1500g/min for 30 min. The obtained serum samples were stored at −80°C until analysis. Enzyme-linked immunosorbent assay determined the level of serum NO in a microplate reader (Synergy 2, BioTek Inc.) by using a commercial NO (NO$_2$/NO$_3$) research kit (catalog no. ADI-917-010, Enzo Life Sciences Inc.).

H$_2$O$_2$ assay
The H$_2$O$_2$ released from bone marrow cells was monitored using Amplex Red Hydrogen Peroxide/Peroxidase Assay kit according to the manufacturer's protocol (catalog no. A22188, Thermo Fisher Scientific Inc.) and a microplate reader (Synergy 2, BioTek Inc.). The positive control was cells stimulated with PMA at a concentration of 100 ng/ml in the presence or absence of 1 mM L-NAME.

Processing of skin cells
Skin sheets from the diseased mouse paws were processed as described previously using collagenase D digestion and deoxyribonuclease I (2). Single-cell suspensions from these skin biopsies were subjected to flow cytometric analyses.

Cytometric beads array
Cytokine levels in the skin culture supernatant were measured by flow cytometry using BD Cytometric Bead Array Mouse/Rat Soluble protein Master Buffer kit (IL-1α, TNF-α, and IL-17A) according to the manufacturer's instruction. Briefly, 2×10^5 skin cells were isolated from the naïve and mannan-immunized mice, which were stimulated with PMA (100 ng/ml) and ionomycin (1 μg/ml) for 4 hours at 37°C.

Flow cytometry
Flow cytometry was performed on single-cell suspensions from skin and peritoneal lavage. The cell sample was stained with a LIVE/DEAD Fixable Dead Cell Stain (catalog no. L10119, Thermo Fisher Scientific Inc.). After an anti-mouse CD16/CD32 Fc block, extracellular antigens were stained for 20 min at 4°C in PBS with 1% fetal bovine serum. For intracellular NOS2 staining, cells were fixed and permeabilized using BD Cytofix/Cytoperm solution (catalog no. 554714, BD Biosciences). For intracellular RORγt staining, cells were fixed and permeabilized by Foxp3/transcription factor fixation/permeabilization concentrate and diluent solutions (catalog no. 00-5521-00, eBioscience) and permeabilization buffer (catalog no. 00-8333-56, eBioscience). Samples were acquired using a BD LSR II flow cytometer operated by DIVA software (BD Biosciences), and the data were analyzed using FlowJo software (TreeStar Inc.).

Tomographic reconstruction
The steady-state SP$_3$ model could be used to describe the light propagation with the wavelength λ, when signals on the surface were acquired from 3D domain of object Ω. Here, $g = 0.90$, and the skin index of refraction was set as 1.40. The absorption coefficient, scattering coefficient, and anisotropic coefficient of each tissue are shown in Table 1 (16). The objective function with the Tikhonov parameter $\alpha = 10^{-6}$ was established by the finite element method

$$J = \frac{1}{2}\int_{\partial\Omega}\left|\varphi(\lambda) - B(\lambda)\right|^2 dr + \frac{\alpha}{2}\int_{\Omega}\left|S(\lambda)\right|^2 dr \quad (1)$$

where φ(λ) is the composite moments relevant to the Legendre moments of the radiance in Ω. Construction of Lagrangian

$$L(\varphi, S, \theta) = J - f(\varphi, \theta) - \int_{\Omega}S(\lambda)\theta\, dr \quad (2)$$

$$\begin{cases} L_{\varphi}'(\varphi, S, \theta)(\gamma) = \int_{\partial\Omega}(\varphi - B)\gamma\, dr - f'(\gamma, \theta) = 0 \\ L_{S}'(\varphi, S, \theta)(\zeta) = \alpha\int_{\Omega}\zeta \cdot S\, dr + \int_{\Omega}\zeta \cdot \theta\, dr = 0 \\ L_{\theta}'(\varphi, S, \theta)(\eta) = -f'(\varphi, \eta) + \int_{\Omega}S \cdot \eta\, dr = 0 \end{cases} \quad (3)$$

The strong form of S(λ) equation

$$\theta = -\alpha S \quad (4)$$

Replace θ with S and construct the following equation into the matrix form by the finite element method

$$\begin{bmatrix} A_{\partial\Omega} & \alpha P^{-1} \\ \alpha M^{-1} & -\alpha A_{\Omega} \end{bmatrix} \begin{bmatrix} \varphi \\ S \end{bmatrix} = \begin{bmatrix} A_{\partial\Omega} \cdot B \\ 0 \end{bmatrix} \quad (5)$$

where P is derived from M after swapping M_{12} and M_{21}. The detailed expression for M can be found in the study of Zhong et al. (16). In addition, here

$$\begin{cases} A_{\partial\Omega} = \int_{\partial\Omega} v_i \cdot v_j \, dr \\ A_\Omega = \int_\Omega v_i \cdot v_j \, dr \end{cases} \quad (6)$$

so that

$$S(\lambda, r, t) = [\alpha P^{-1} + A_{\partial\Omega} M A_s]^{-1} A_{\partial\Omega} B(\lambda, r, t) \quad (7)$$

$S(\lambda, r, t)$ denotes the solution in the global space, which stands for the time-dependent concentration of light-emitting source inside heterogeneous tissues.

The 4-view optical scanning and x-ray data were fused into a finite element mesh of 15,747 nodes, 113,940 triangles, and 49,152 tetrahedrons. The number of surface nodes was 7051. The mean user time per sample was 152 min in total when the whole program was implemented on the computer of Macmini 5.2, Intel Core i5 @ 2.50GHz, 8.0 GB RAM.

Statistics

All statistical analyses were evaluated by Mann-Whitney U test (Graph Prism software, version 6.0h). $P < 0.05$ was considered as significant. *$P < 0.05$, **$P < 0.01$, ***$P < 0.001$, and ****$P < 0.0001$.

SUPPLEMENTARY MATERIALS

Supplementary material for this article is available at http://advances.sciencemag.org/cgi/content/full/4/5/eaas9864/DC1

fig. S1. Representative flow cytometry gating scheme for NOS2 expression analysis in human IFN-γ/LPS–activated MDSCs and in vitro–differentiated TIP DCs.
fig. S2. Representative flow cytometry gating scheme for skin ILC3 analysis at the paw.
fig. S3. Representative flow cytometry gating scheme for skin γδ T cells analysis at the paw.

REFERENCES AND NOTES

1. T. T. Jiang, T.-Y. Shao, W. X. G. Ang, J. M. Kinder, L. H. Turner, G. Pham, J. Whitt, T. Alenghat, S. S. Way, Commensal fungi recapitulate the protective benefits of intestinal bacteria. Cell Host Microbe 22, 809–816.e4 (2017).
2. I. Khmaladze, T. Kelkka, S. Guerard, K. Wing, A. Pizzolla, A. Saxena, K. Lundqvist, M. Holmdahl, K. S. Nandakumar, R. Holmdahl, Mannan induces ROS-regulated, IL-17A–dependent psoriasis arthritis-like disease in mice. Proc. Natl. Acad. Sci. U.S.A. 111, E3669–E3678 (2014).
3. B. L. S. Picciani, B. Michalski-Santos, S. Carneiro, A. L. Sampaio, J. C. R. Avelleira, D. R. Azulay, J. M. N. Pinto, E. P. Dias, Oral candidiasis in patients with psoriasis: Correlation of oral examination and cytopathological evaluation with psoriasis disease severity and treatment. J. Am. Acad. Dermatol. 68, 986–991 (2013).
4. E. W. Rosenberg, P. W. Belew, Microbial factors in psoriasis. Arch. Dermatol. 118, 143–144 (1982).
5. W.-H. Boehncke, M. P. Schön, Psoriasis. Lancet 386, 983–994 (2015).
6. J. Knight, S. L. Spain, F. Capon, A. Hayday, F. O. Nestle, A. Clop; Wellcome Trust Case Control Consortium; Genetic Analysis of Psoriasis Consortium; I-chip for Psoriasis Consortium, J. N. Barker, M. E. Weale, R. C. Trembath, Conditional analysis identifies three novel major histocompatibility complex loci associated with psoriasis. Hum. Mol. Genet. 21, 5185–5192 (2012).
7. S. Pantelyushin, S. Haak, B. Ingold, P. Kulig, F. L. Heppner, A. A. Navarini, B. Becher, Rorγt+ innate lymphocytes and γδ T cells initiate psoriasiform plaque formation in mice. J. Clin. Invest. 122, 2252–2256 (2012).
8. F. Villanova, B. Flutter, I. Tosi, K. Grys, H. Sreeneebus, G. K. Perera, A. Chapman, C. H. Smith, P. Di Meglio, F. O. Nestle, Characterization of innate lymphoid cells in human skin and

9. blood demonstrates increase of NKp44+ ILC3 in psoriasis. J. Invest. Dermatol. 134, 984–991 (2014).
9. J. Bowes, A. Budu-Aggrey, U. Huffmeier, S. Uebe, K. Steel, H. L. Hebert, C. Wallace, J. Massey, I. N. Bruce, J. Bluett, M. Feletar, A. W. Morgan, H. Marzo-Ortega, G. Donohoe, D. W. Morris, P. Helliwell, A. W. Ryan, D. Kane, R. B. Warren, E. Korendowych, G.-M. Alenius, E. Giardina, J. Packham, R. McManus, O. FitzGerald, N. McHugh, M. A. Brown, P. Ho, F. Behrens, H. Burkhardt, A. Reis, A. Barton, Dense genotyping of immune-related susceptibility loci reveals new insights into the genetics of psoriatic arthritis. Nat. Commun. 6, 6046 (2015).
10. P. E. Stuart, R. P. Nair, L. C. Tsoi, T. Tejasvi, S. Das, H. M. Kang, E. Ellinghaus, V. Chandran, K. Callis-Duffin, R. Ike, Y. Li, X. Wen, C. Enerbäck, J. E. Gudjonsson, S. Kõks, T. Kingo, T. Esko, U. Mrowietz, A. Reis, H. E. Wichmann, C. Gieger, P. Hoffmann, M. M. Nöthen, J. Winkelmann, M. Kunz, E. G. Moreta, P. J. Mease, C. T. Ritchlin, A. M. Bowcock, G. G. Krueger, H. W. Lim, S. Weidinger, M. Weichenthal, J. J. Voorhees, P. Rahman, P. K. Gregersen, A. Franke, D. D. Gladman, G. R. Abecasis, J. T. Elder, Genome-wide association analysis of psoriatic arthritis and cutaneous psoriasis reveals differences in their genetic architecture. Am. J. Hum. Genet. 97, 816–836 (2015).
11. D. J. Stuehr, M. A. Marletta, Mammalian nitrate biosynthesis: Mouse macrophages produce nitrite and nitrate in response to Escherichia coli lipopolysaccharide. Proc. Natl. Acad. Sci. U.S.A. 82, 7738–7742 (1985).
12. S. Guerard, R. Holmdahl, K. Wing, Reactive oxygen species regulate innate but not adaptive inflammation in ZAP70-mutated SKG arthritic mice. Am. J. Pathol. 186, 2353–2363 (2016).
13. K. A. Gelderman, M. Hultqvist, A. Pizzolla, M. Zhao, K. S. Nandakumar, R. Mattsson, R. Holmdahl, Macrophages suppress T cell responses and arthritis development in mice by producing reactive oxygen species. J. Clin. Invest. 117, 3020–3028 (2007).
14. J. Zhong, L. M. Olsson, V. Urbonaviciute, M. Yang, L. Bäckdahl, R. Holmdahl, Association of NOX2 subunits genetic variants with autoimmune diseases. Free Radic. Biol. Med. https://doi.org/10.1016/j.freeradbiomed.2018.03.005 (2018).
15. L. M. Olsson, Å. C. Johansson, B. Gullstrand, A. Jönsen, L. Saevarsdottir, L. Rönnblom, D. Leonard, J. Wetterö, C. Sjöwall, E. Svenungsson, I. Gunnarsson, A. A. Bengtsson, R. Holmdahl, A single nucleotide polymorphism in the NCF1 gene leading to reduced oxidative burst is associated with systemic lupus erythematosus. Ann. Rheum. Dis. 76, 1607–1613 (2017).
16. J. Zhong, J. Tian, X. Yang, C. Qin, Whole-body Cerenkov luminescence tomography with the finite element SP₃ method. Ann. Biomed. Eng. 39, 1728–1735 (2011).
17. A. Kielland, T. Blom, K. S. Nandakumar, R. Holmdahl, R. Blomhoff, H. Carlsen, In vivo imaging of reactive oxygen and nitrogen species in inflammation using the luminescent probe L-012. Free Radic. Biol. Med. 47, 760–766 (2009).
18. K. Van Dyke, E. Ghareeb, M. Van Dyke, D. H. Van Thiel, Ultrasensitive peroxynitrite-based luminescence with L-012 as a screening system for antioxidative/antinitrating substances, e.g. Tylenol (acetaminophen), 4-OH tempol, quercetin and carboxy-PTIO. Luminescence 22, 267–274 (2007).
19. V. E. Laubach, E. G. Shesely, O. Smithies, P. A. Sherman, Mice lacking inducible nitric oxide synthase are not resistant to lipopolysaccharide-induced death. Proc. Natl. Acad. Sci. U.S.A. 92, 10688–10692 (1995).
20. N. V. Serbina, T. P. Salazar-Mather, C. A. Biron, W. A. Kuziel, E. G. Pamer, TNF/iNOS-producing dendritic cells mediate innate immune defense against bacterial infection. Immunity 19, 59–70 (2003).
21. D. Wilsmann-Theis, S. Koch, C. Mindnich, S. Bonness, S. Schnautz, D. von Bubnoff, T. Bieber, Generation and functional analysis of human TNF-α/iNOS-producing dendritic cells (Tip-DC). Allergy 68, 890–898 (2013).
22. C. Guo, F. Hu, H. Yi, Z. Feng, C. Li, L. Shi, Y. Li, H. Liu, X. Yu, H. Wang, J. Li, Z. Li, X.-Y. Wang, Myeloid-derived suppressor cells have a proinflammatory role in the pathogenesis of autoimmune arthritis. Ann. Rheum. Dis. 75, 278–285 (2016).
23. S. Mandruzzato, S. Brandau, C. M. Britten, V. Bronte, V. Damuzzo, C. Gouttefangeas, D. Maurer, C. Ottensmeier, S. H. van der Burg, M. J. P. Welters, S. Walter, Toward harmonized phenotyping of human myeloid-derived suppressor cells by flow cytometry: Results from an interim study. Cancer Immunol. Immunother. 65, 161–169 (2016).
24. J. Bagaitkar, N. K. Pech, S. Ivanov, A. Austin, M. Y. Zeng, S. Pallat, G. Huang, G. J. Randolph, M. C. Dinauer, NADPH oxidase controls neutrophilic response to sterile inflammation in mice by regulating the IL-1α/G-CSF axis. Blood 126, 2724–2733 (2015).
25. C. Garlanda, C. A. Dinarello, A. Mantovani, The interleukin-1 family: Back to the future. Immunity 39, 1003–1018 (2013).
26. C. C. Winterbourn, Reconciling the chemistry and biology of reactive oxygen species. Nat. Chem. Biol. 4, 278–286 (2008).
27. H. Vu-Quang, M. Muthiah, Y.-K. Kim, C.-S. Cho, R. Namgung, W. J. Kim, J. H. Rhee, S. H. Kang, S. Y. Jun, Y.-J. Choi, Y. Y. Jeong, I.-K. Park, Carboxylic mannan-coated iron oxide nanoparticles targeted to immune cells for lymph node-specific MRI in vivo. Carbohydr. Polym. 88, 780–788 (2012).
28. K. Sato, X.-l. Yang, T. Yudate, J.-S. Chung, J. Wu, K. Luby-Phelps, R. P. Kimberly, D. Underhill, P. D. Cruz Jr., K. Ariizumi, Dectin-2 is a pattern recognition receptor for fungi that couples

with the Fc receptor γ chain to induce innate immune responses. *J. Biol. Chem.* **281**, 38854–38866 (2006).

29. C. Hagert, O. Sareila, T. Kelkka, S. Jalkanen, R. Holmdahl, The macrophage mannose receptor regulate mannan-induced psoriasis, psoriatic arthritis, and rheumatoid arthritis-like disease models. *Front. Immunol.* **9**, 114 (2018).

30. D. T. Brody, S. K. Durum, Membrane IL-1: IL-1 alpha precursor binds to the plasma membrane via a lectin-like interaction. *J. Immunol.* **143**, 1183–1187 (1989).

31. S. Koide, R. M. Steinman, Induction of murine interleukin 1: Stimuli and responsive primary cells. *Proc. Natl. Acad. Sci. U.S.A.* **84**, 3802–3806 (1987).

32. K. Shimizu, A. Nakajima, K. Sudo, Y. Liu, A. Mizoroki, T. Ikarashi, R. Horai, S. Kakuta, T. Watanabe, Y. Iwakura, IL-1 receptor type 2 suppresses collagen-induced arthritis by inhibiting IL-1 signal on macrophages. *J. Immunol.* **194**, 3156–3168 (2015).

33. F. Obermeier, V. Gross, J. Schölmerich, W. Falk, Interleukin-1 production by mouse macrophages is regulated in a feedback fashion by nitric oxide. *J. Leukoc. Biol.* **66**, 829–836 (1999).

34. A. Akitsu, H. Ishigame, S. Kakuta, S.-h. Chung, S. Ikeda, K. Shimizu, S. Kubo, Y. Liu, M. Umemura, G. Matsuzaki, Y. Yoshikai, S. Saijo, Y. Iwakura, IL-1 receptor antagonist-deficient mice develop autoimmune arthritis due to intrinsic activation of IL-17-producing CCR2$^+$Vγ6$^+$γδ T cells. *Nat. Commun.* **6**, 7464 (2015).

35. H. Rabeony, M. Pohin, P. Vasseur, I. Petit-Paris, J.-F. Jégou, L. Favot, E. Frouin, M.-A. Boutet, F. Blanchard, D. Togbe, B. Ryffel, F.-X. Bernard, J.-C. Lecron, F. Morel, IMQ-induced skin inflammation in mice is dependent on IL-1R1 and MyD88 signaling but independent of the NLRP3 inflammasome. *Eur. J. Immunol.* **45**, 2847–2857 (2015).

36. K. M. Coleman, J. E. Gudjonsson, M. Stecher, Open-label trial of MABp1, a true human monoclonal antibody targeting interleukin 1α, for the treatment of psoriasis. *JAMA Dermatol.* **151**, 555–556 (2015).

37. A. Ali, M. Na, M. N. D. Svensson, A. Magnusson, A. Welin, J.-C. Schwarze, M. Mohammad, E. Josefsson, R. Pullerits, T. Jin, IL-1 receptor antagonist treatment aggravates staphylococcal septic arthritis and sepsis in mice. *PLOS ONE* **10**, e0131645 (2015).

38. N. Jung, M. Hellmann, R. Hoheisel, C. Lehmann, I. Haase, A. Perniok, M. Hallek, A. Rubbert, An open-label pilot study of the efficacy and safety of anakinra in patients with psoriatic arthritis refractory to or intolerant of methotrexate (MTX). *Clin. Rheumatol.* **29**, 1169–1173 (2010).

39. C. Bogdan, Nitric oxide synthase in innate and adaptive immunity: An update. *Trends Immunol.* **36**, 161–178 (2015).

40. W. Taylor, D. Gladman, P. Helliwell, A. Marchesoni, P. Mease, H. Mielants; CASPAR Study Group, Classification criteria for psoriatic arthritis: Development of new criteria from a large international study. *Arthritis Rheum.* **54**, 2665–2673 (2006).

Citation: J. Zhong, T. Scholz, A. C. Y. Yau, S. Guerard, U. Hüffmeier, H. Burkhardt, R. Holmdahl, Mannan-induced Nos2 in macrophages enhances IL-17–driven psoriatic arthritis by innate lymphocytes. *Sci. Adv.* **4**, eaas9864 (2018).

ScienceAdvances

Mannan-induced Nos2 in macrophages enhances IL-17−driven psoriatic arthritis by innate lymphocytes

Jianghong Zhong, Tatjana Scholz, Anthony C. Y. Yau, Simon Guerard, Ulrike Hüffmeier, Harald Burkhardt and Rikard Holmdahl

ARTICLE TOOLS	http://advances.sciencemag.org/content/4/5/eaas9864
SUPPLEMENTARY MATERIALS	http://advances.sciencemag.org/content/suppl/2018/05/14/4.5.eaas9864.DC1
REFERENCES	This article cites 39 articles, 10 of which you can access for free http://advances.sciencemag.org/content/4/5/eaas9864#BIBL
PERMISSIONS	http://www.sciencemag.org/help/reprints-and-permissions

Use of this article is subject to the Terms of Service